Chapter 4

Nature of Magnetic Ordering in Cobalt-Based Spinels

Subhash Thota and Sobhit Singh

Additional information is available at the end of the chapter

http://dx.doi.org/10.5772/65913

Abstract

In this chapter, the nature of magnetic ordering in cobalt-based spinels Co_3O_4, Co_2SnO_4, Co_2TiO_4, and Co_2MnO_4 is reviewed, and some new results that have not been reported before are presented. A systematic comparative analysis of various results available in the literature is presented with a focus on how occupation of the different cations on the A- and B-sites and their electronic states affect the magnetic properties. This chapter specifically focuses on the issues related to (i) surface and finite-size effects in pure Co_3O_4, (ii) magnetic-compensation effect, (iii) co-existence of ferrimagnetism and spin-glass-like ordering, (iv) giant coercivity (H_C) and exchange bias (H_{EB}) below the glassy state, and (v) sign-reversal behavior of H_{EB} across the ferri/antiferromagnetic Néel temperature (T_N) in Co_2TiO_4 and Co_2SnO_4. Finally, some results on the low-temperature anomalous magnetic behavior of Co_2MnO_4 spinels are presented.

Keywords: ferrimagnetic materials, Néel temperature, spin-glass, exchange bias

1. Introduction

The atomic arrangement of the spinel compounds is interpreted as a pseudo-close-packed arrangement of the oxygen anions with divalent cations occupying tetrahedral A-sites and trivalent cations residing at the octahedral B-sites of the cubic unit cell of space group Fd-3m(227). A spinel with the configuration (A^{2+}) $[B_2^{3+}]$ O_4 is termed as "normal spinel" whereas the other possible configuration (B^{3+}) $[A^{2+}B^{3+}]$ O_4 is called "inverse spinel." The continuum of possible atomic distribution between these two extremes is quantified by a parameter denoted as x (inversion parameter), which describes the fraction of "B" cations on tetrahedral sites. Thus, $x = 0$ for a normal spinel, 2/3 for a spinel with entirely arbitrary configuration, and 1 for a fully inverse spinel. Among many varieties of spinel compounds,

ferrites and cobaltites are widely used in the high-frequency electronic circuit components such as transformers, noise filters, and magnetic recording heads [1, 2]. The key property of these spinels is that at high frequencies (>1 MHz), their dielectric permittivity (ε) and magnetic permeability (μ) are much higher than those of metals with low loss-factor (tanδ). These properties make them very advantageous for the development of magnetic components used in the power electronics industry. Also, the nanostructures of these spinels continue to receive large attention because of their potential applications in solid-oxide fuel cells, Li-ion batteries, thermistors, magnetic recording, microwave, and RF devices [1, 2].

In this review, we mainly focus on the nature of magnetic ordering of several insulating cobalt spinels of type Co_2MO_4 (where "M" is the tetravalent or trivalent metal cation such as Sn, Ti, Mn, Si, etc.) which are not yet well studied in literature. This review will primarily illustrate how the magnetic ordering changes when we substitute the above-listed metal cations at the tetrahedral B-sites. It is well known that the dilution of magnetic elements significantly disrupts the long-range magnetic ordering and leads to more exotic properties like magnetic frustration, polarity reversal exchange bias, and reentrant spin-glass state near the magnetic-phase transition [3, 4]. The dilution essentially alters the super-exchange interactions of J_{AB}, J_{BB}, and J_{AA} between the magnetic ions, which is the main source of anomalous magnetic behavior. In this review, we first start with the simplest case of antiferromagnetic (AFM) normal-spinel Co_3O_4 with configuration $(Co^{2+})[Co_2^{3+}]O_4$ and discuss the role of surface and finite-size effects on antiferromagnetic (AFM) ordering. In the second section, we focus on the coexistence of ferrimagnetism and low-temperature spin-glass behavior of cobalt orthostannate (Co_2SnO_4) and cobalt orthotitanate (Co_2TiO_4). A detailed comparative analysis of some recent experimental results dealing with the temperature and frequency dependence of ac-magnetic susceptibility is presented. In the subsequent section, some unusual magnetic properties of Co_2MnO_4 are discussed.

2. Magnetic properties of bulk versus nanocrystalline Co_3O_4

Cobalt forms two binary compounds with oxygen: CoO and Co_3O_4. While CoO has face-centered cubic (NaCl-type) structure, Co_3O_4 shows a normal-spinel structure with a cubic close packed arrangement of oxygen ions and Co^{2+} and Co^{3+} ions occupying the tetrahedral "8a" and the octahedral "16d" sites, respectively [5]. The magnetic properties of Co_3O_4 were first investigated over 58 years ago; however, its magnetic behavior under reduced dimensions still attracted immense scientific interest mainly because of its distinctly different magnetic ordering under nanoscale as compared to its bulk counterpart [6]. Co_3O_4 can be synthesized in various nanostructural forms such as nanorods, nanosheets, and ordered nanoflowers with ultrafine porosity [7–10]. Such engineered nanostructures play vital roles as catalysts, gas sensors, magneto-electronics, electrochromic devices, and high-temperature solar selective absorbers [11–18]. At first glance, the normal-spinel structure of Co_3O_4 may look similar to that of Fe_3O_4 (inverse spinel) but Co_3O_4 exhibits strikingly different magnetic ordering as compared to Fe_3O_4. In particular, Co_3O_4 does not exhibit ferrimagnetic ordering of the type observed in Fe_3O_4 because Co^{3+} ions on the octahedral B-sites are in the low spin $S = 0$ state [5].

Instead, it exhibits antiferromagnetic ordering with each Co^{2+} ion at the A-site having four neighboring Co^{2+} ions of opposite spins (with an effective magnetic moment of $\mu_{eff} \sim 4.14\ \mu_B$) [5]. Earlier studies by Roth reported that below the Néel temperature $T_N \sim 40$ K, Co_3O_4 becomes antiferromagnetic in which the uncorrelated spins of the $8Co^{2+}$ (in 8(a), F.C. +000, $\frac{1}{4}\frac{1}{4}\frac{1}{4}$) cations in the paramagnetic state (space group O^7_h—Fd-3m) are split in the antiferromagnetic state (space group T^2_d—F$\bar{4}$3m) into the two sublattices with oppositely directed spins of $4Co^{2+}\uparrow$ (4(a), +000) and $4Co^{2+}\downarrow$ (4(c) $\frac{1}{4}\frac{1}{4}\frac{1}{4}$) [5–7]. For $T < T_N$, the neutron diffraction studies did not show any evidence of a structural phase transition.

As shown in **Figure 1**, the recent magnetic studies by Dutta et al. [6] have reported a significant difference in the antiferromagnetic ordering temperature $T_N \sim 30$ K of Co_3O_4 as compared to the earlier data (40 K); this new result however is in excellent agreement with $T_N = 29.92 \pm 0.03$ K obtained by the heat capacity C_p versus T measurements reported by Khriplovich et al. [19]. It is well known that the peak in the magnetic susceptibility data of antiferromagnets usually occurs at a temperature few percent higher than T_N because the magnetic specific heat of a simple antiferromagnet (in particular, the singular behavior in the region of the transition) should be closely similar to the behavior of the function $d(\chi_p T)/dT$ [14]. Therefore, T_N is better

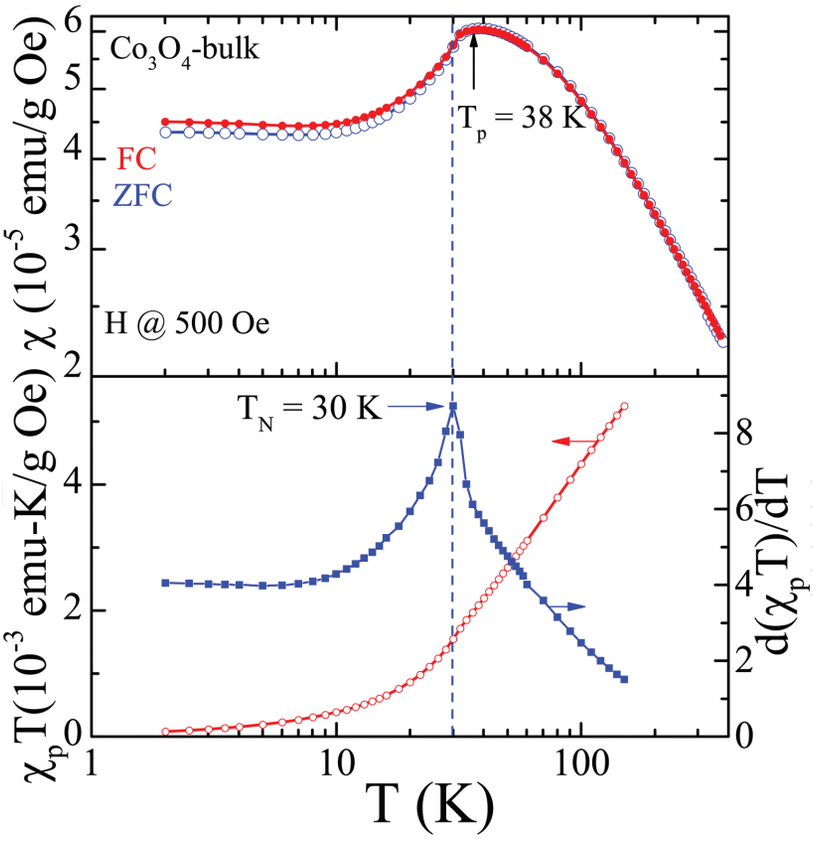

Figure 1. (a) Temperature dependence of the dc-magnetic susceptibility $\chi(T)$ for bulk Co_3O_4 under the zero-field-cooled (ZFC) and field-cooled (FC) conditions. Here, T_p denotes the peak position in χ versus T plots. (b) Plots of $(\chi_p T)$ versus T (LHS scale) and $d(\chi_p T)/dT$ versus T plots (RHS scale) for the bulk Co_3O_4. Here, the paramagnetic susceptibility $\chi_p = \chi - \chi_0$ with $\chi_0 = 3.06 \times 10^{-6}$ emu/g Oe being the temperature-independent contribution [6, 7].

defined by the peak in $\partial(\chi T)/\partial T$ versus T plot [20]. **Figure 1** shows the temperature dependence of paramagnetic susceptibility $\chi_p(T)$ (LHS scale) and $d(\chi_p T)/dT$ versus T (RHS scale). For bulk Co_3O_4 the peak temperature value (30 K) in the $d(\chi_p T)/dT$ versus T plots is lower than $T_N \simeq 40$ K often quoted for Co_3O_4 [5–7, 9–10]. Thus, $T_N = 30$ K determined from two independent techniques (i.e., χ_p and C_p measurements) is consistent with each other and is the accurate characteristic value for bulk Co_3O_4. On the other hand, the nanoparticles of Co_3O_4 exhibit lower T_N values and reduced magnetic moment than the bulk value (30 K, 4.14 μ_B) which is a consequence of finite-size and surface effects [6]. Salabas et al. first reported Co_3O_4 nanowires of diameter 8 nm and lengths of up to 100 nm by the nanocasting route and observed $T_B \simeq 30$ K and exchange bias (H_e) for $T < T_B$ [10].

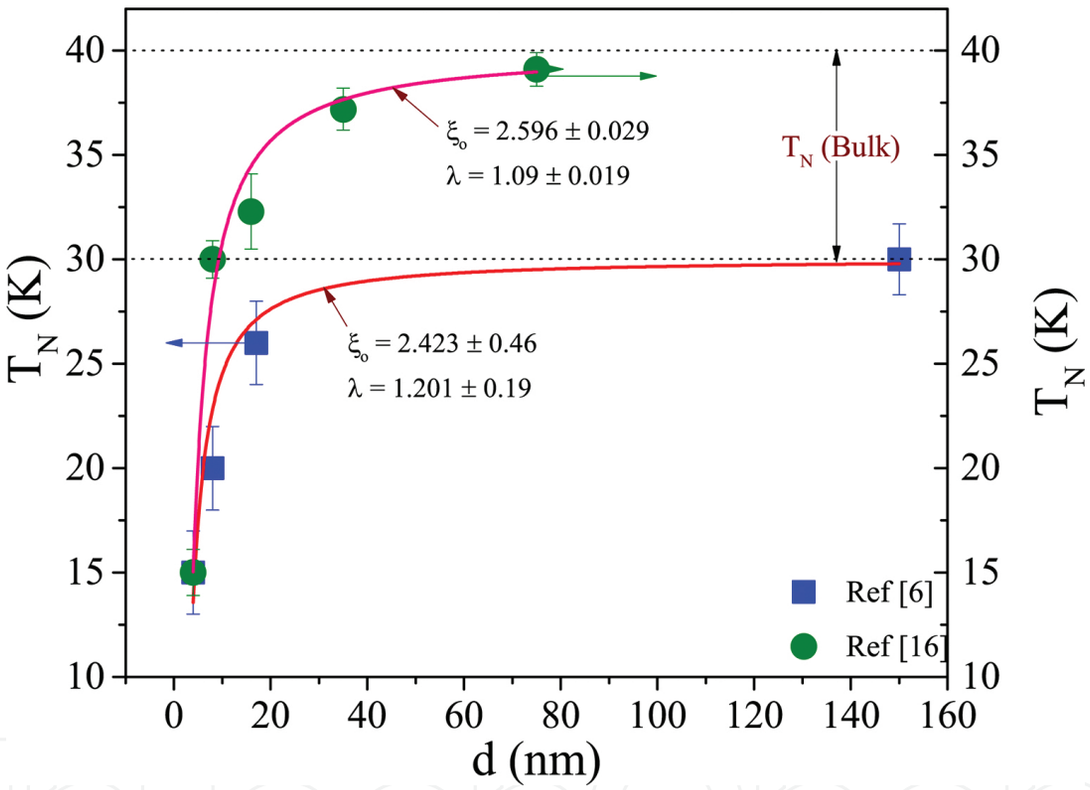

Figure 2. Variation of the Néel temperature T_N of Co_3O_4 as a function of particle size (d). The data pertaining to solid-square symbols are taken from Refs. [6–8] in which T_N is considered as a peak point in"$d(\chi_p T)/dT$" versus"T" data. However, the data related to solid green circles are taken from Refs. [8, 9] in which T_N is considered as just the peak point in the "χ"versus"T" plot, not from the derivative plots. The scattered symbols are the raw data corresponding to T_N and the solid lines are the best fit to Eq. (1).

A plot of T_N values versus particle size d reported by several authors for various crystallite sizes of Co_3O_4 is shown in **Figure 2**. The lowest T_N value reported till now is about 15 ± 2 K for 4.34 nm size Co_3O_4 particles [8]. These nanoparticles were synthesized using biological containers of Listeria innocua Dps proteins and LDps as constraining vessels. Lin and Chen studied the magnetic properties of various sizes (diameter d = 16, 35, and 75 nm) of Co_3O_4 nanoparticles prepared by chemical methods using $CoSO_4$ and $CoCl_2$ as precursors [9]. These authors reported that the variation of T_N follows the finite-size scaling relation:

http://dx.doi.org/10.5772/65913

$$T_N(D) = T_N(\infty)\left[1 - \left(\frac{\xi_0}{d}\right)^{\lambda}\right] \quad (1)$$

for various sizes of Co_3O_4 nanoparticles. Accordingly, they obtained the shift exponent $\lambda = 1.1 \pm 0.2$ and the correlation length $\xi_o = 2.8 \pm 0.3$ nm from the fitting analysis of T_N versus d (**Figure 2**). However, these authors considered T_N values as the direct peak temperature values from χ versus T instead of the peak point in $d(\chi_p T)/dT$. Also, for the bulk grain sizes $T_N(\infty) = 40$ K was considered instead of 30 K obtained from $d(\chi_p T)/dT$ analysis as discussed above. Therefore, we repeated the analysis but considering T_N values obtained from $d(\chi_p T)/dT$ versus T and the $T_N(\infty) = 30$ K for various sizes of the Co_3O_4 nanoparticles obtained by sol-gel process (these values were obtained from our earlier works [6, 7]). Accordingly, we obtained $\lambda = 1.201 \pm 0.2$ and the correlation length $\xi_o = 2.423 \pm 0.46$ nm, which are slightly different from the earlier reported values $\lambda = 1.1 \pm 0.2$ and the correlation length $\xi_o = 2.8 \pm 0.3$ nm [9]. Nonetheless, in both the cases T_N follows the finite-size scaling relation Eq. (1).

For $T > T_N$, the data of χ versus T (**Figure 3**) are fitted to the modified Curie-Weiss law $\chi_P = \chi_0 + [C/(T+\theta)]$ with $C = N\mu^2/3k_B$, $\mu^2 = g^2 J(J+1)\mu_B^2$, θ is the Curie-Weiss temperature and χ_0 contains two contributions: the temperature-independent orbital contribution mentioned earlier and

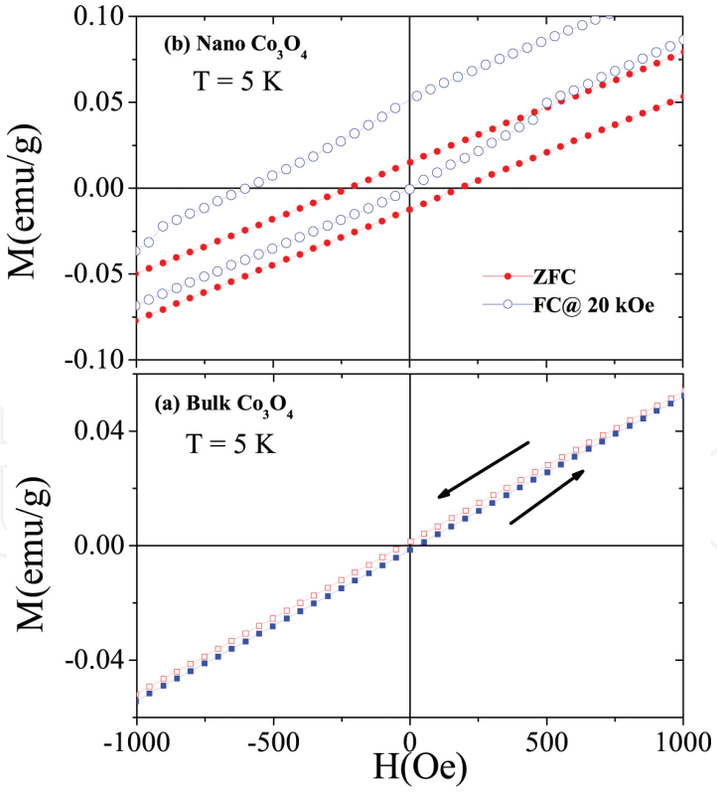

Figure 3. $1/\chi_p$ versus T plots for the bulk and nanocrystalline (~17 nm) Co_3O_4 with $\chi_0 = 3.06 \times 10^{-6}$ emu/g Oe (LHS scale). The solid lines represent linear fit to the Curie-Weiss law: $\chi_p = C/(T + \theta)$. On the RHS scale same figures are plotted except for $\chi_0 = 9 \times 10^{-6}$ and 7.5×10^{-6} emu/g Oe for the bulk and Co_3O_4 nanoparticles of size ~17 nm, respectively [6, 7].

the diamagnetic component $\chi_d = -3.3 \times 10^{-7}$ emu/g Oe [6]. Usually χ_0 is estimated from the plot of χ versus $1/T$ in the limit of $1/T \rightarrow 0$ using the high-temperature data. The value of χ_0 was estimated as 3.06×10^{-6} emu/g Oe for bulk Co_3O_4 using the inverse paramagnetic susceptibility ($1/\chi_P$) versus temperature (T) data (shown in the left-hand-side scale of **Figure 3**) [5, 6]. A similar procedure for experimental data, shown in the right-hand side scale of **Figure 3**, yields $\chi_0 = 9 \times 10^{-6}$ and 7.5×10^{-6} emu/g Oe for the bulk and nanoparticles (size ~17 nm) of Co_3O_4, respectively.

It is well known that the origin of the antiferromagnetic ordering in transition metal oxides can be explained by the super-exchange interaction between the magnetic elements via oxygen ion. In the present case, there are two possible paths for super-exchange interaction between magnetic ions in Co_3O_4, i.e., Co^{2+} ions: (tetrahedral site) A – O (oxygen) – A (tetrahedral site) and A – O – B – O – A with the number of nearest-neighbors $z_1 = 4$ and next-nearest-neighbors $z_2 = 12$, respectively. If the corresponding exchange constants are represented by J_{1ex} and J_{2ex}, the expressions for T_N and θ, using the molecular-field theory, can be written as [5, 6]

$$T_N = \frac{J(J+1)}{3k_B}\left(J_{1ex}z_1 - J_{2ex}z_2\right) \tag{2}$$

$$\theta = \frac{J(J+1)}{3k_B}\left(J_{1ex}z_1 + J_{2ex}z_2\right) \tag{3}$$

In order to determine J_{1ex} and J_{2ex}, the magnitude of effective $J(J + 1)$ for Co^{2+} is required. Since the Curie constant C is equivalent to $N\mu^2/3k_B$ with $\mu = g\,[J(J + 1)]^{1/2}\mu_B$ where g is the Landé g-factor and J is the total angular momentum. Using the magnitude of $g = 2$ and C from **Figure 3**, one can estimate the effective magnetic moment $\mu_{eff} = 4.27\mu_B$ for bulk Co_3O_4 and $\mu = 4.09\mu_B$ for Co_3O_4 nanoparticles of size ~17 nm. The spin contribution to the above magnitudes of μ is $3.87\mu_B$ for Co^{2+} with spin $S = 3/2$. Obviously, there is some additional contribution resulting from the partially restored orbital angular moment for the $^4F_{9/2}$ ground state of Co^{2+} [5, 6]. Using Eqs. (2) and (3) and the values of "θ," "T_N," and "μ" for the two cases yields $J_{1ex} = 11.7$ and $J_{2ex} = 2.3$ K for bulk, and $J_{1ex} = 11.5$ and $J_{2ex} = 2.3$ K for the Co_3O_4 nanoparticles (d ~ 17 nm). Thus, both the exchange constants J_{1ex} and J_{2ex} correspond to antiferromagnetic coupling. From the magnitudes of C in **Figure 3**, the value of μ is obtained as 3.28 and 3.43 μ_B for bulk and Co_3O_4 nanoparticles (d ~17 nm), respectively. These magnitudes of μ are lower than the spin contribution (3.87 μ_B) of Co^{2+} ion itself. Consequently, the magnitudes of "θ" in **Figure 3** seem to be questionable. This may be due to the fact that the use of molecular-field theory in determining the exchange constants has its own limitations since higher order spin correlations are neglected in this model [6].

For a typical bulk antiferromagnet, below T_N, the magnetization is expected to vary linearly with applied external magnetic field H below the spin-flop field. Therefore, the corresponding coercive field H_c and exchange-bias field H_e must become zero. This was indeed observed in bulk Co_3O_4 (**Figure 4a**) [5, 6]. Conversely, for the Co_3O_4 nanoparticles (d ~ 17 nm), the data at

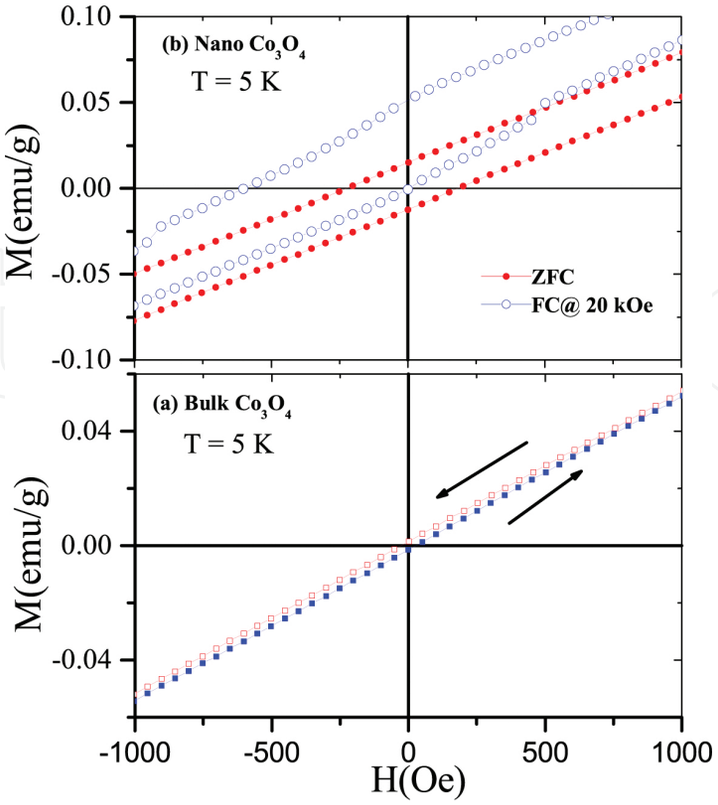

Figure 4. The magnetization (M) versus external applied field (H) plots recorded in standard five-cycle hysteresis mode for bulk and nanoparticles (d ~17 nm) of Co_3O_4 measured at 5 K in the lower field region of ±1 kOe. (a) Irreversibility observed for the direct and reverse field scans for bulk Co_3O_4, however, (b) a asymmetric shift in the hysteresis loop with enhanced coercivity can be clearly noticed in the case of nanoparticles (d ~ 17 nm) of Co_3O_4 measured under field-cooled protocol (FC) of H = 20 kOe [6, 7].

5 K show a symmetric hysteresis loop with H_c = 200 Oe for the zero-field-cooled sample and asymmetric (shifted) hysteresis loop with H_c = 250 Oe and H_e = −350 Oe for the sample cooled in magnetic field H = 20 kOe from 300 to 5 K as shown in **Figure 4b**. Thus, cooling the sample in a magnetic field produces an exchange bias and leads to the enhancement of H_c as well. The temperature dependence of H_c and H_e for the nanoparticles of Co_3O_4 cooled under H = 20 kOe from 300 K to the measuring temperature is shown in **Figure 5**. Both H_c and H_e approach to zero above T_N. The inset of **Figure 5** depicts the training effect, i.e., change in the magnitude of H_e for the sample cycled through several successive hysteresis loops (designated by "n" at 5 K) [6, 10]. A similar effect has been recently reported by Salabas et al. [10] in the Co_3O_4 nanowires of 8 nm diameter although the magnitudes of H_e and H_c in their case are somewhat smaller. The existence of the exchange bias suggests the presence of a ferromagnetic (shell)/antiferromagnetic (core) interface with FM-like surface spins covering the core of the antiferromagnetically ordered spins in the nanoparticles of Co_3O_4. Salabas et al. reported that H_e falls by ~25% measured between the first and the second loops. The observation of the training effect and open loops of up to 55 kOe suggests that the surface spins are in an unstable spin-glass-like state [10]. Such a spin-glass ordering results from the weaker exchange coupling experienced by the surface spins due to reduced coordination at the surface. These effects however disappear above T_N when the spins in the core become disordered. The observation

of somewhat lower magnetic moment per Co^{2+} ion, smaller values of exchange constants J_{1ex} and J_{2ex}, and lower T_N was noticed for the nanoparticles of Co_3O_4 in relation to the bulk Co_3O_4. This could be due to the weak exchange coupling and reduced coordination of the surface spins.

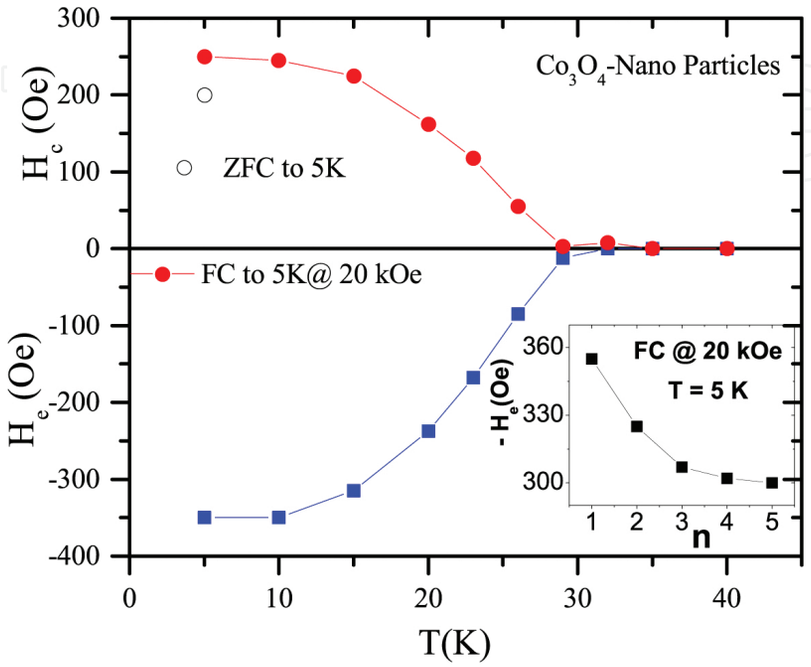

Figure 5. The temperature dependence of H_c and H_e for the nanoparticles of Co_3O_4 ($d \sim 17$nm) measured from $T = 5$ to 40 K under field-cooled (FC) mode at 20 kOe and at 5 K under zero-field-cooled (ZFC) condition [6]. One can clearly notice $H_c \rightarrow 0$, $H_e \rightarrow 0$ as T approaches T_N. The inset shows progressive decrease of the magnitude of H_e after successive scan (number of cycles"n") at 5 K [6].

3. Co-existence of ferrimagnetism and spin-glass states in some inverted spinels

In 1975, Sherrington and Kirkpatrick (SK) first predicted the reentrant behavior of spinels using mean-field approach for certain relative values of the temperature and exchange interaction [21, 22]. Later, Gabay and Toulouse extended the SK Ising model calculation to the vector spin glasses and showed that it is possible to have multiple phase transitions such as ferro/ferri/antiferromagnetic state $\overset{T_C \text{ or } T_N}{\longleftrightarrow}$ paramagnetic state $\overset{T_{M1}}{\longleftrightarrow}$ Mixed phase-1 $\overset{T_{M2}}{\longleftrightarrow}$ Mixed phase-2 [22, 23]. The present section deals with such kind of systems in which the longitudinal ferrimagnetic ordering coexists with the transverse spin-glass state below the Néel temperature T_N [23–28]. In this connection, we mainly focus on the magnetic ordering in two inverse-spinel systems, namely (i) cobalt orthostannate (Co_2SnO_4) and (ii) cobalt orthotitanate (Co_2TiO_4) which exhibits the reentrant spin-glass behavior [24–40]. At first glimpse, both systems Co_2SnO_4 and Co_2TiO_4 are expected to show similar magnetic properties because of the fact that

nonmagnetic ions Sn and Ti play identical role on the global magnetic ordering of the system. But in reality, they exhibit markedly different magnetic structures below their ferrimagnetic Néel temperatures [24–40], which is discussed in detail below.

Usually, the ferrimagnetic ordering in Co_2SnO_4 and Co_2TiO_4 arises from the unequal magnetic moments of Co^{2+} ions at the tetrahedral A-sites and octahedral B-sites [24–40]. The corresponding magnetic moment at the tetrahedral A-sites μ(A) is equal to 3.87 μ_B and the magnetic moment at octahedral B-sites μ(B) is equal to 5.19 and 4.91 μ_B for Co_2TiO_4 and Co_2SnO_4, respectively [27–33]. In 1976, Harmon et al. first reported the low-temperature magnetic properties of polycrystalline Co_2SnO_4 system and showed the evidence for ferrimagnetic ordering with $T_N \sim 44 \pm 2$ K [24]. They also suggested that Co_2SnO_4 should contain two equally populated sublattices that align collinearly and couple antiferromagnetically [24]. On the basis of the Mössbauer spectroscopy results, these authors calculated the internal dipolar fields at the Sn sites from the two Co^{2+} sublattices to be > 80 kOe [24]. They also reported very high values of coercive field $H_C > 50$ kOe below T_N [24]. The reported magnetization value at 16 K per Co^{2+} ion was about 2.2×10^{-3} μ_B with zero magnetization value at 12 K. The Curie-Weiss constant (C) = 4.3 ± 0.2 emu/mol, and the effective magnetic moment of the Co^{2+} ions = 5.0 ± 0.2 μ_B was close to the standard value of 4.13 emu/mol and 4.8 μ_B, respectively. A year later, Sagredo et al. reported that the zero-field-cooled and field-cooled magnetization curves of single crystal Co_2SnO_4 exhibit strong irreversibility below T_N [39].

Sagredo et al. reported that thermoremanent magnetization, magnetic training effects, and spin-glass phases present in this system are driven by the disordered-spin configurations [39]. Accordingly, they speculated that the random distribution of Sn^{4+} ions on the B-sites might break the octahedral symmetry of the crystal field and result in the frustrated magnetic behavior [39]. In 1987, Srivastava et al. reported multiple peaks in the temperature dependence of ac-magnetic susceptibility $\chi_{ac}(T)$ for both Co_2SnO_4 and Co_2TiO_4 below their T_N providing the evidence of Gabay and Tolouse mixed-phase transitions [25, 28]. Nevertheless, some recent studies proved the existence of transverse spin-glass state T_{SG} (~39 K) just below the T_N (= 41 K) in Co_2SnO_4 [27, 38, 40]. Similar type of results in Co_2TiO_4 was reported by Hubsch et al. and Srivastava et al. but with different T_{SG} (~46 K) and T_N (=55 K) [25, 28, 31, 34].

In order to get a precise understanding of the magnetic properties of these systems, we have plotted the temperature dependence of dc-magnetic susceptibility $\chi_{dc}(T)$ for both Co_2SnO_4 and Co_2TiO_4 measured under ZFC and FC (H@100 Oe) conditions in **Figure 6**. These $\chi_{dc}(T)$ plots show typical characteristics of ferrimagnetic ordering with peaks across the Néel temperatures T_N = 47 K (for Co_2TiO_4) and 39 K (for Co_2SnO_4). However, for $T \leq 31.7$ K an opposite trend in the $\chi_{dc}(T)$ values was noticed for Co_2TiO_4 with $\chi_{dc} \sim 0$ at magnetic-compensation temperature T_{CMP} = 31.7 K at which the two-bulk sublattices magnetizations completely balances with each other [31–33]. Such compensation behavior in Co_2SnO_4 system is expected to appear at very low temperatures ($T < 10$ K) as $\chi_{dc}(T)$ approaches to zero. Consequently, $\chi_{dc\text{-}ZFC}$ exhibits negative magnetization until $T_{SG.}$ It is expected that the different magnetic moments on the tetrahedral (A) and the octahedral (B) sites, and their different temperature dependence (i.e., $\mu_A(T)$, $\mu_B(T)$) play a major role on the global magnetic ordering of both systems.

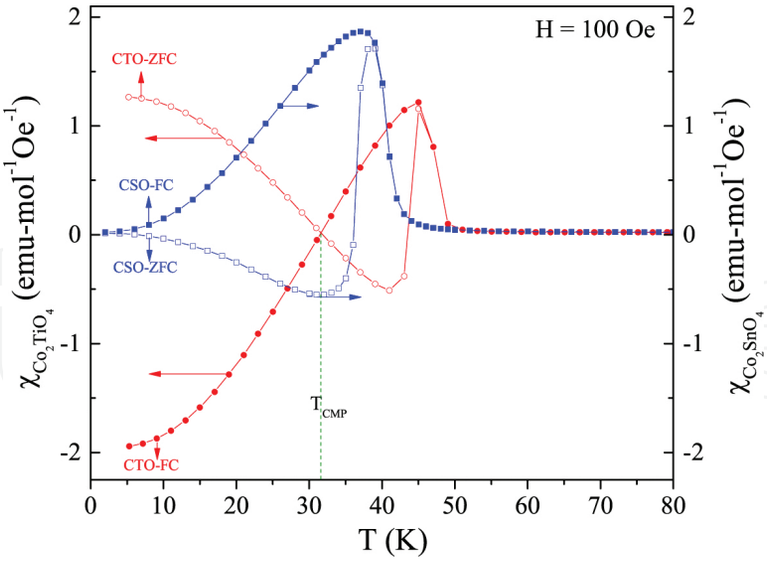

Figure 6. The temperature dependence of dc-magnetic susceptibility $\chi_{dc}(T)$ measured under ZFC and FC (H@100 Oe) conditions for both Co_2TiO_4 (LHS) and Co_2SnO_4 (RHS). The dotted line shows the T_{CMP}.

Recent X-ray photoelectron spectroscopic studies reveal that the crystal structure of Co_2TiO_4 consists of some fraction of trivalent cobalt and titanium ions at the octahedral sites, i.e., $[Co^{2+}][Co^{3+}Ti^{3+}]O_4$ instead of $[Co^{2+}][Co^{2+}Ti^{4+}]O_4$ [34]. On the contrary, the Co_2SnO_4 shows the perfect tetravalent nature of stannous ions without any trivalent signatures of Co^{3+} $[Co^{2+}][Co^{2+}Sn^{4+}]O_4$ [27]. Such distinctly different electronic structure of the ions on the B-sites of cobalt orthotitanate plays a significant role on the anomalous magnetic ordering below T_N, for example, exhibiting the magnetic-compensation behavior, sign reversible zero-field exchange-bias, and negative slopes in the Arrott plots (H/M versus M^2) [27, 34].

At high temperatures (for all $T > T_N$), the experimental data of inverse dc-magnetic susceptibility (χ^{-1}) for both the systems Co_2TiO_4 and Co_2SnO_4 fit well with the modified Néel expression for ferrimagnets $(1/\chi) = (T/C) + (1/\chi_0) - [\sigma_0/(T - \theta)]$. **Table 1** summarizes various fitting parameters obtained from the Néel expression for both Co_2SnO_4 and Co_2TiO_4. The fit for Co_2TiO_4 yields the following parameters: $\chi_0 = 41.92 \times 10^{-3}$ emu/mol-Oe, $\sigma_0 = 31.55$ mol-Oe-K/emu, $C = 5.245$ emu K/mol Oe, $\theta = 49.85$ K. The ratio $C/\chi_0 = T_a = 125.1$ K represents the strength of the antiferromagnetic exchange coupling between the spins on the A- and B-sites and is often termed as the asymptotic Curie temperature T_a. For both the systems, the effective magnetic moment μ_{eff} is determined from the formula $C = N\mu_{eff}^2/3k_B$. The experimentally observed magnetic moments at the B-sites $\mu(B) = 5.19$ μ_B obtained from the temperature dependence of magnetization values are in line with the above-discussed spectroscopic properties of Co_2TiO_4, i.e., the total moment $\mu(B)$ is perfectly matching with the contribution from the magnetic moments due to Co^{3+} (4.89 μ_B) and Ti^{3+} (1.73 μ_B), $\mu(B) = \sqrt{\left(\mu_{Co}+3\right)^2 + \left(\mu_{Ti}+3\right)^2}$ [34]. Also, the analysis of the dc and ac susceptibilities combined with the weak anomalies observed in the C_p versus T data has shown the existence of a quasi-long-range ferrimagnetic state below $T_N \sim 47.8$ K and a compensation temperature of $T_{CMP} \sim 32$ K [34].

System	C (emu K/mol/Oe)	χ_o (emu/mol/Oe)	σ_o (Oe mol K emu^{-1})	θ (K)	μ_{eff} (μ_B)	μ (A) (μ_B)	μ(B) (μ_B)
Co_2TiO_4	5.245	0.0419	31.55	49.85	6.5	3.87	5.19
		N_{AA}	N_{AB}	N_{BB}	J_{AA}	J_{AB}	J_{BB}
		17.319	35.700	12.720	3.25 k_B	4.47 k_B	3.18 k_B
Co_2SnO_4	4.889	0.0436	102.370	39.5	6.25	3.87	4.91
		N_{AA}	N_{AB}	N_{BB}	J_{AA}	J_{AB}	J_{BB}
		21.564	33.201	10.68	4.05 k_B	5.26 k_B	4.28 k_B

Table 1. The list of various parameters obtained from the Néel fit of χ^{-1} versus T curve recorded under zero-field-cooled condition.

The real and imaginary components of the temperature dependence of ac-susceptibility data $\chi_{ac}(T)$ (= $\chi'(T) + i\,\chi''(T)$) recorded at different frequencies for both the polycrystalline samples Co_2SnO_4 and Co_2TiO_4 show the dispersion in their peak positions ($T_P(f)$) similar to the compounds exhibiting spin-glass-like ordering [27, 33]. **Figure 8** shows the $\chi'(T)$ and $\chi''(T)$ data of Co_2SnO_4 and Co_2TiO_4 recorded at different measuring frequencies ranging from 0.17 to 1202 Hz with peak-to-peak field amplitude H_{ac} = 4 Oe under zero dc-bias field. It is clear from these figures that the peaks seen in both cases show pronounced frequency dependence, which suggests the dynamical features analogous to that of observed in spin-glass systems. A detailed analysis of such frequency dependence of $\chi'(T)$ and $\chi''(T)$ using two scaling laws described below provides the evidence for spin-glass-like characteristics below T_N. For example, applying the Vogel-Fulcher law (below equation) for interacting particles

$$\tau = \tau_0 \exp\left(\frac{E_a}{k_B\left(T - T_0\right)}\right) \tag{4}$$

and the best fits of the experimental data (the logarithmic variation of relaxation time"τ" as a function of $1/(T_F - T_0)$ as shown in **Figure 8a** yields the following parameters: interparticle interaction strength T_0 = 39.3 K and relaxation time constant $\tau_0 = 7.3 \times 10^{-8}$ s for Co_2SnO_4. Here, we define the freezing temperature for each frequency is T_F, angular frequency ω as $2\pi f$ ($\omega = 1/\tau$), k_B is the Boltzmann constant, and E_a is an activation energy parameter. Such large value of τ_0 indicates the presence of interacting magnetic spin clusters of significant sizes in the polycrystalline Co_2SnO_4 system. The origin of such spin clusters may arise from a short-range magnetic order occurring due to the competition between ferrimagnetism and magnetic frustration. Another characteristic feature that the spin-glass systems follows is the power law (Eq. (5)) of critical slowing down in a spin-glass phase transition at T_{SG} (note that the $T_P(f)$ data represent a relatively small temperature interval):

$$\tau = \tau_0\left(\frac{T}{T_g} - 1\right)^{-z\upsilon} \tag{5}$$

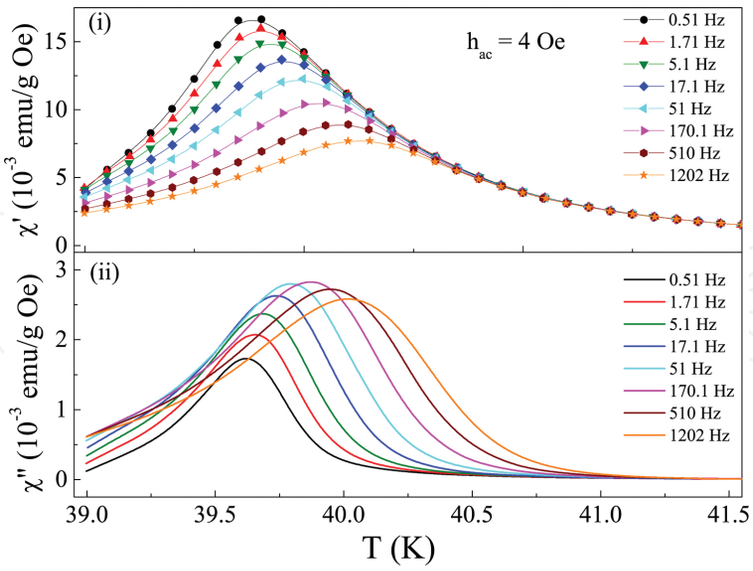

Figure 7(a). The temperature dependence of the ac-magnetic susceptibilities (i) real $\chi'(T)$ component and (ii) imaginary $\chi''(T)$ component of bulk polycrystalline Co_2SnO_4 system recorded at various frequencies under warming condition using dynamic magnetic field of amplitude h_{ac} = 4 Oe and zero static magnetic field H_{dc} = 0. The lines connecting the data points are visual guides [27].

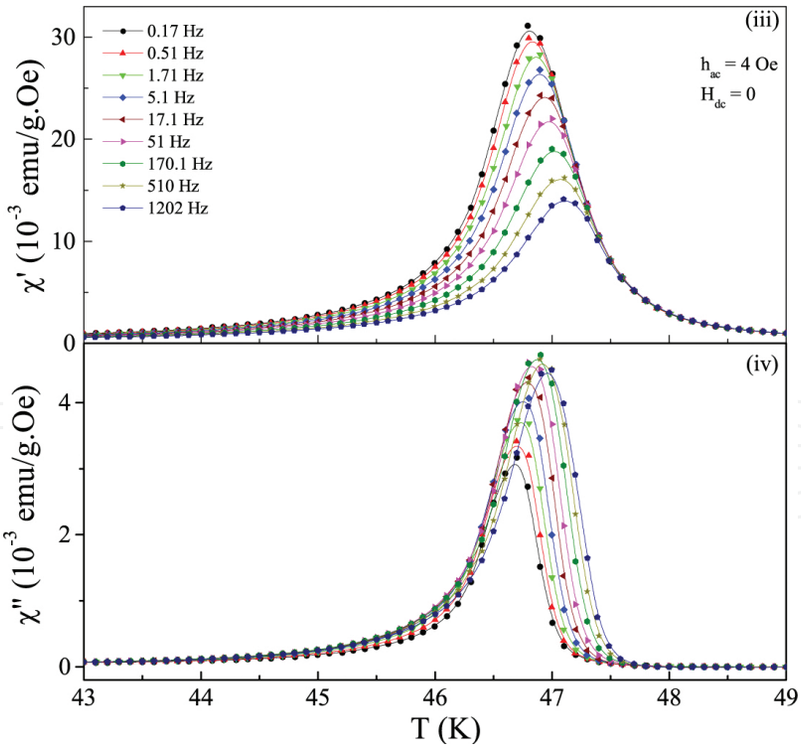

Figure 7(b). The temperature dependence of the ac-magnetic susceptibilities (iii) real $\chi'(T)$ component and (iv) imaginary $\chi''(T)$ component of bulk polycrystalline Co_2TiO_4 system recorded at various frequencies under warming condition using dynamic magnetic-field of amplitude h_{ac} = 4 Oe and zero static magnetic field H_{dc} = 0. The lines connecting the data points are visual guides [33].

The least-square fit using the power law of the data shown in **Figure 7** is depicted in **Figure 8b**. Here, T_{SG} is the freezing temperature, τ_0 is related to the relaxation of the individual cluster magnetic moment, and $z\nu$ is a critical exponent. The least-square fit analysis for Co_2SnO_4 gives $T_{SG} = 39.6$ K, $\tau_0 = 1.4 \times 10^{-15}$ s, and $z\nu = 6.4$. Since the value of $z\nu$ obtained in the present case lies well within the range (6–8) of a typical spin-glass systems; thus, one can conclude that Co_2SnO_4 exhibits spin-glass-like phase transition across 39 K just below the $T_N \sim 41$ K [20, 27]. In these studies, the difference in T_0 and T_{SG} is very small (~0.3 K) suggesting the close resemblance between the current Co_2SnO_4 system and the compounds exhibiting spin-glass-like transition. However, the situation for Co_2TiO_4 is bit different; in particular, the best fit to the Vogel-Fulcher law yields $T_0 = 45.8$ K and $\tau_0 = 3.2 \times 10^{-16}$ s and the power law yielded fairly unphysical values of the fitting parameters: for example, $\tau_0 \sim 10^{-33}$ s with $z\nu > 16$, indicating the lack of spin-glass-like phase transition [33]. Although, the magnitude and shift of the ac-susceptibility values both $\chi'(T)$ and $\chi''(T)$ strongly suppressed in the presence of dc-magnetic field (H_{DC}) in a similar way as it occurs in a typical spin-glass system perfectly following the linear behavior of $H^{2/3}$ versus T_P (AT-line analysis). Under such tricky situation, it is very difficult to conclude that Co_2TiO_4 is a perfect spin-glass or not (of course one can call it as a pseudo-spin-glass system). Nevertheless, the ac-magnetic susceptibility data and its analysis suggested that the both Co_2SnO_4 and Co_2TiO_4 systems consist of interacting magnetic clusters close to a spin-glass state.

Another interesting feature of both Co_2SnO_4 and Co_2TiO_4 is that they show asymmetry in M-H hysteresis loops unveiling giant coercivities and bipolar exchange bias under both ZFC and FC cases below their T_N [27, 31, 33]. Earlier studies by Hubsch et al. have shown unusual temperature dependence of coercive field $H_C(T)$ in polycrystalline Co_2TiO_4 sample where the M-H loops were measured in 20-kOe field at different temperatures below 60 K [31]. It is well known that the discovery of exchange-bias (H_{EB}) effect in the structurally single-phase materials with mixed magnetic phases has recently gained tremendous attention because of its technological applications in the development of Read/Write heads of the magnetic

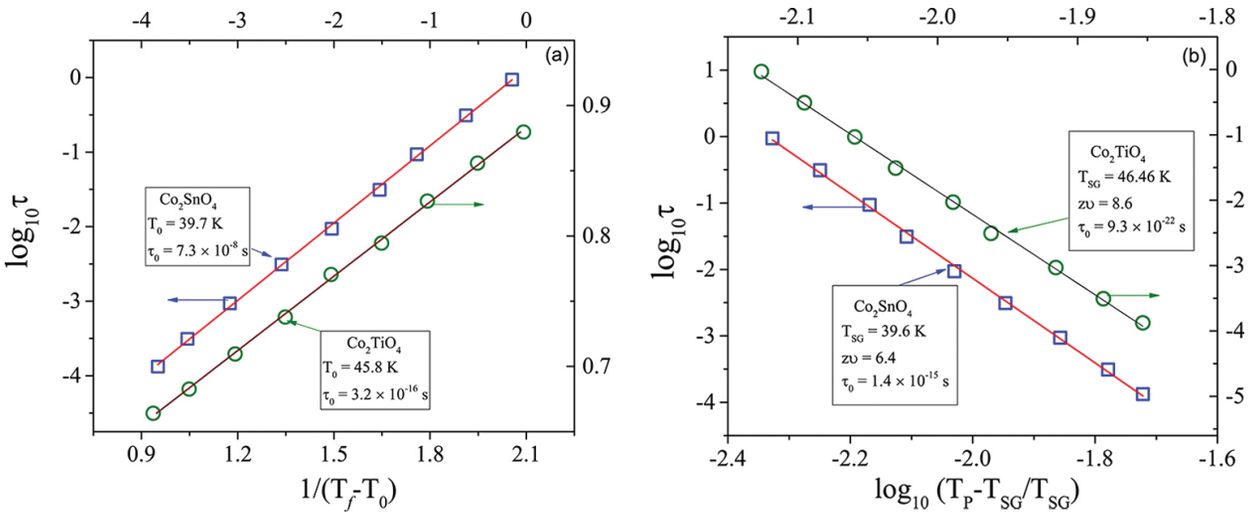

Figure 8. The best fit of the relaxation times to the (a) Vogel-Fulcher law and the (b) power law for the spinels Co_2SnO_4 and Co_2TiO_4.

recording devices [41]. Generally, H_{EB} has been experimentally observed only in the systems cooled in the presence of external magnetic field (FC mode) from above the Néel temperature or spin-glass freezing point. Such systems usually comprise of variety of interfaces such as ferromagnetic (FM)-antiferromagnetic (AFM), FM-SG, FM-ferrimagnetic, AFM-ferrimagnetic, and AFM-SG [41–49]. However, few recent papers have reported significant H_{EB} even under the zero-field-cooled samples of bulk Ni-Mn-In alloys and in bulk Mn_2PtGa [48, 49]. The source of such unusual H_{EB} under zero-field-cooled sample was attributed to the presence of complex magnetic interfaces such as ferrimagnetic/spin-glass or AFM/spin-glass phases [48–51]. Some recent reports have suggested that large exchange anisotropy can originate from the exchange interaction between the compensated host and ferromagnetic clusters [48–51]. Strikingly, Hubsch et al. observed the $H_C \rightarrow 0$ anomalies across T_{CMP}, T_{SG}, and T_N in the temperature-dependent data of H_C for Co_2TiO_4 samples [31]. Slightly different results were reported by Nayak et al. in Ref. [33], where H_C values drops monotonically on approaching T_N. However, the behavior of temperature dependence of exchange-bias field $H_{EB}(T)$ and remanent magnetization $M_R(T)$ in Ref. [33] closely resembles with the trend of $H_C(T)$ reported by Hubsch et. al. in polycrystalline Co_2TiO_4 samples. On the other hand, the temperature behavior of $H_{EB}(T)$, $H_C(T)$, and $M_R(T)$ in Co_2SnO_4 is way different from that of Co_2TiO_4 though they are isostructural with each other. It is likely that the different magnitudes and different temperature dependences of the moments on the Co^{2+} ions on the "A"- and "B"-sites in Co_2SnO_4 are responsible for the anomalous behavior in the $H_{EB}(T)$, $H_C(T)$, and $M_R(T)$ observed below T_N. Moreover, in Co_2SnO_4 below about 15 K, the data suggest that there is nearly complete effective balance of the antiferromagnetically coupled Co^{2+} moments at the"A"- and"B"-sites leading to negligible values of H_C and M_R.

Results from neutron diffraction in Co_2TiO_4 suggested the presence of canted-spins, likely resulting from magnetic frustration caused by the presence of nonmagnetic Ti^{4+} ions on the"B"-sites. A similar canting of the spins might be present in Co_2SnO_4 although neutron diffraction studies are needed to verify this suggestion [27, 31, 33]. Other Co-based spinel compounds that display the reversal in the orientation of the magnetic moments along with negative magnetization due to the magnetic-compensation phenomena are $CoCr_2O_4$ and $Co(Cr_{0.95}Fe_{0.05})_2O_4$ [3, 52, 53].

4. Magnetic properties of bulk and nanocrystalline Co_2MnO_4

Among various Co_2XO_4 (X = Mn, Ni, Co, Zn, etc.) spinels, Co_2MnO_4 has retained a unique place. In particular, Mn- and Co-based spinel oxides have gained considerable interest in the recent past due to their numerous applications in the Li-ion batteries [54, 55], sensors [56–58], thermistors [59], energy-conversion devices [60], and as a catalyst for the reduction of nitrogen oxides [61]. Moreover, Co_2MnO_4 nanocrystals have demonstrated outstanding catalytic properties for oxygen reduction reaction (ORR) and oxygen evolution reaction (OER) [60]. ORR and OER are the essential reactions in the electrochemistry-based energy-storage and energy-conversion devices. Co_2MnO_4 has shown superior catalytic activities compared to the commercial 30 wt% platinum supported on carbon black (Pt/C). Due to the special surface

morphology [62], Co_2MnO_4 spinel is a very promising pseudo-capacitor material [63, 64]. Co_2MnO_4 has also demonstrated potential applications for protective coating on ferrite stainless steel interconnects in solid-oxide fuel cells (SOFCs) [65, 66]. Furthermore, colossal magnetoresistance (CMR) has been observed in the Mn- and Co-based spinel oxides [67].

In addition to the novel catalytic properties, Co_2MnO_4 spinel exhibits intriguing magnetic properties. Lotgering first observed the existence of ferromagnetic ordering in Co_2MnO_4 spinels [68]. Ríos et al. systematically studied the effect of Mn concentration on the magnetic properties of $Co_{3-x}Mn_xO_4$ solid solutions prepared by spray pyrolysis [69]. As we have discussed in Section 2 that Co_3O_4 has an antiferromagnetic order with T_N = 30 K. When we replace Co in Co_3O_4 by Mn cation, large ferromagnetic ordering appears, which ultimately dominates the antiferromagnetic ordering at x = 1. Therefore, pure Co_2MnO_4 shows ferromagnetic behavior and this has been confirmed by detailed magnetic measurements [70, 71]. However, for value of x other than 0 (Co_3O_4) and 1 (Co_2MnO_4), both ferromagnetic and antiferromagnetic magnetic exchange interactions coexist in the system, which yields a ferrimagnetic ordering in the $Co_{3-x}Mn_xO_4$ ($0 < x < 1$) solid solutions [72]. Tamura performed pressure-dependent study of Curie temperature (T_C) and found that T_C decreases with increase in pressure [71].

Pure Co_2MnO_4 possess a cubic inverse-spinel structure: $(B^{3+})[A^{2+}B^{3+}]O_4$ (shown in **Figure 9**). In an ideal case, the octahedral [B] sites are occupied by divalent cations together with half of the trivalent cations and the rest of the trivalent cations occupy the tetrahedral (A) sites in the spinel structure. However, due to the presence of different oxidation states of Mn and Co cations at (A) and [B] sites, the actual cationic distribution of Co_2MnO_4 is very complex and it has been a topic of considerable debate [59, 70–84]. Different sample preparation conditions also play an important role in the cationic distribution of Co_2MnO_4. On the basis of X-ray diffraction, electrical conductivity, magnetic, physiochemical, and neutron diffraction measurements, several different cationic distributions for nonstoichiometric $Co_{3-x}Mn_xO_4$ ($0 < x < 1$) have been reported in literature [59, 70–84]. From the magnetic measurements, Wickham and Croft proposed the following cationic distribution: $Co^{2+}[Co_{2-x}^{3+}Mn_x^{3+}]O_4 (0 < x < 2)$ for solid solutions of $Co_{3-x}Mn_xO_4$ systems obtained after the thermal decomposition of co-precipitated manganese and cobalt salts [72]. Later studies by Blasse suggested a different cationic distribution: $Co^{2+}[Co_{2-x}^{2+}Mn_x^{4+}]O_4$ [73]. Based on the physicochemical properties, Ríos et al. proposed a more complicated cationic distribution: $Co_{0.88}^{2+}Mn_{0.12}^{2+}[Co_{0.87}^{3+}Co_{0.22}^{2+}Mn_{0.09}^{3+}Mn_{0.76}^{4+}\blacksquare_{0.06}]O_4$ for Co_2MnO_4 powder samples prepared by thermal decomposition of nitrate salts [74]. From the neutron diffraction and magnetic measurements, Boucher et al. reported the cationic distribution $Co^{2+}[Co_{2-x}^{3+}Mn_x^{3+}]O_4$ similar to the one reported by Wickham and Croft [72, 75]. Yamamoto et al. [76] performed neutron diffraction measurements on Co_2MnO_4 oxides prepared by chemical methods at low temperatures, and reported $Mn_{1-n}Co_n[Mn_xCo_{2-n}]O_4$ as atomic distribution. Here, n is the inversion parameter of the inverse-spinel structure. Gautier et al. suggested two different possible cationic distributions: $Co^{2+}[Co^{3+}Mn_{0.35}^{2+}Mn_{0.29}^{3+}Mn_{0.36}^{4+}]O_4$ and

$Co^{2+}[Co^{3+}_{0.95}Mn^{2+}_{0.015}Mn^{3+}_{0.50}Mn^{4+}_{0.485}\blacksquare_{0.05}]O_4$ [77, 78]. On the contrary, the electrical conductivity measurements suggest a different cationic distribution: $Co^{2+}[Co^{2+}_{x}Co^{3+}_{2(1-x)}Mn^{4+}_{x}]O_4$, and $Co^{2+}[Co^{2+}Mn^{4+}]O_4$ or $Co^{3+}[Co^{3+}Mn^{2+}]O_4$ [59, 79] for Co_2MnO_4 spinel. Aoki studied the phase diagram and cationic distribution of various compositions of manganese and cobalt mixed spinel oxides [80]. He further investigated the effect of temperature and Mn concentration on the structure of manganese-cobalt spinel oxide systems. Control over morphology, crystallite site, grain size, and specific surface area of Co_2MnO_4 powders can be achieved by thermal decomposition of precursors in a controlled atmosphere [81, 82].

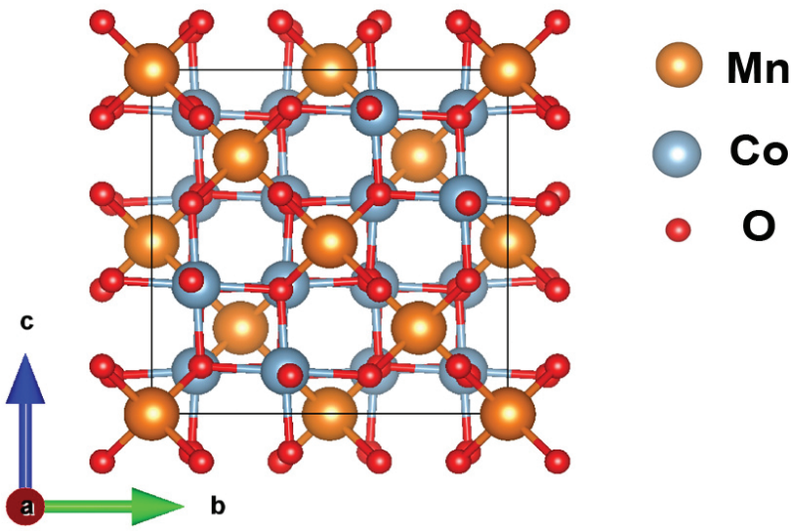

Figure 9. Cubic inverse-spinel structure of Co_2MnO_4 in Fd-3m (227) space group.

In 2008, Bazuev et al. investigated the effect of oxygen stoichiometry on the magnetic properties of $Co_2MnO_{4+\delta}$ [83]. Accordingly, two oxygen-rich compositions, (i) $Co_2MnO_{4.62}$ and (ii) $Co_2MnO_{4.275}$, were prepared by the thermal decomposition of presynthesized Co and Mn binary oxalates ($Mn_{1/3}Co_{2/3}C_2O_4 \cdot 2H_2O$). Above studies also report existence of anomalous behavior in the magnetic properties of $Co_2MnO_{4.275}$ spinel at low temperatures and high magnetocrystalline anisotropy in $Co_2MnO_{4.62}$. Bazuev et al. also noticed that T_N of $Co_2MnO_{4+\delta}$ is highly sensitive to the oxygen stoichiometry, imperfections in the cationic sublattice and variation in the Mn oxidation states. The imperfect $Co_2MnO_{4+\delta}$ inherits ferrimagnetic ordering that arises due to the antiferromagnetic exchange between Co^{2+} ($e_g^4 t_{2g}^3$) and Mn^{4+} ($t_{2g}^3 e_g^0$)) cations located at the tetrahedral and octahedral sites, respectively. To further investigate the electronic states of Mn and Co cations in the Co_2MnO_4 lattice, Bazuev at al. employed the X-ray absorption near-edge spectroscopy (XANES) to probe the electronic states of the absorbing atoms and their local neighborhood [83]. XANES spectra of both $Co_2MnO_{4.62}$ and $Co_2MnO_{4.275}$ compositions revealed that Co is present in both Co^{2+} and Co^{3+} oxidation states while Mn is present as Mn^{4+} and Mn^{3+}. Additionally, it was found that Mn is located in a higher symmetry octahedral crystal field environment [83]. Bazuev at al. further proposed following cationic

distributions for $Co_2MnO_{4.275}$ and $Co_2MnO_{4.62}$ compositions: $Co^{2+}_{0.936}[Co^{III}_{0.936}Mn^{3+}_{0.421}Mn^{4+}_{0.515}]O_4$ and $Co^{2+}_{0.66}[Mn^{4+}_{0.866}Co^{III}_{1.072}]O_4$, respectively. Here, Co^{III} is a low-spin cation while Co^{2+} and Mn^{3+} are high-spin cations.

Co_2MnO_4 spinels have gained peculiar interest of researchers due to their unusual magnetic hysteresis behavior at low temperatures. Joy and Date [70] first observed the unusual magnetic hysteresis behavior in Co_2MnO_4 nanoparticles below 120 K. By means of the magnetic hysteresis loop measurements at low temperatures, they realized that the initial magnetization curve (virgin curve) lies outside the main hysteresis loop at 120 K. However, for $T > 120$ K, they observed normal hysteresis behavior in Co_2MnO_4. This unusual behavior of hysteresis loop at low temperatures can be associated with the irreversible domain wall motion. At low magnetic fields ($H < H_C$), domain walls experience substantial resistance during their motion with increasing magnetic field. Similar behavior has been observed for some other alloys [85–87]. Such irreversible movement of domain walls was ascribed to the rearrangement of valence electrons at low temperatures. Generally, in a system with mixed oxidation states of Mn at high temperatures, short-range diffusion of Co ions, $Co^{3+} \leftrightarrows Co^{2+}$ associated with $Mn^{3+} \leftrightarrows Mn^{4+}$, gets activated at low temperatures. This may cause change in the local ordering of the ions at the octahedral sites. Consequently, the resistance for domain wall motion increases and this slows down the motion of domain walls. Soon after Joy and Date, Borges et al. [84] confirmed that the unusual hysteresis of Co_2MnO_4 compound indeed arises due to the irreversible domain wall motion. Borges et al. prepared various different size nanoparticles of Co_2MnO_4 by Pechini method and performed the magnetic hysteresis measurements at low temperatures [84]. They observed that the samples below a critical diameter ($d < 39$ nm) exhibit normal hysteresis behavior, while the bulk grain size samples ($d \sim 200$ nm) show unusual hysteresis behavior at low temperatures. Using the spherical particle model, Borges et al. further calculated the critical diameter (d_{cr}) of a single-domain wall in Co_2MnO_4 and obtained that $d_{cr} = 39$ nm [88]. Therefore, all particles with diameter $d < d_{cr}$ can be considered as a single-domain particle. Since particles with $d < d_{cr}$ show normal hysteresis while particles with $d > d_{cr}$ show unusual hysteresis behavior, one can conclude that the unusual hysteresis behavior is indeed due to the irreversible motion of the domain walls.

The dynamic magnetic properties of Co_2MnO_4 nanoparticles of average diameter 28 nm were reported by Thota et al. [89]. A detailed study of dc- and ac-magnetic susceptibility measurements of these nanoparticles reveals the low temperature spin-glass-like characteristics together with the memory and aging effects (**Figure 10**). **Figure 10** shows the temperature dependence of real and imaginary part of the ac-susceptibility ($\chi'(T)$ and $\chi''(T)$) of Co_2MnO_4 nanoparticles recorded at different values of frequencies (f) between 1 Hz and 1.48 kHz at a peak-to-peak amplitude of 1 Oe. Both $\chi'(T)$ and $\chi''(T)$ exhibit a sharp peak at the onset of ferromagnetic ordering ($T_C = T_1 = 176.4$ K) and a broad cusp centered at T_2 ($<T_C$).

The temperature at which both $\chi'(T)$ and $\chi''(T)$ attain the maximum value shifts toward high-temperature side as the frequency increases from 1 Hz and 1.48 kHz similar to spin-glass behavior. Such frequency dependence of $\chi'(T)$ and $\chi''(T)$ follows the Vogel-Fulcher law (Eq. (4) and insets of **Figures 10a(ii)** and **b(ii)**) and power law of critical slowing down (Eq. (5) and

insets of **Figures 10a(i)** and **b(i)**). Least-square fit to these equation yields the following parameters (insets of **Figure 10**): interparticle interaction strength (T_0) = 162 K for T_1 (118 K for T_2) and relaxation time constant $\tau_0 = 6.18 \times 10^{-15}$ s for T_1 (4.4×10^{-15} s for T_2), critical exponent ($z\nu$) = 6.01 for T_1 (7.14 for T_2), and spin-glass transition temperature (T_{SG}) = 162.6 K for T_1 (119.85 K for T_2). Since the values of $z\nu$ for both the peaks T_1 and T_2 of Co_2MnO_4 nanoparticles lie well within the range (6–8) of a typical spin-glass systems, one can conclude that Co_2MnO_4 exhibits spin-glass-like phase transition across 162.6 K just below the $T_C \sim 176.4$ K [89]. **Figure 11a** shows the magnetization relaxation of Co_2MnO_4 nanoparticles under ZFC and FC protocols with a temperature quench to 70 K at H = 250 Oe [89]. The magnetization relaxation during the third cycle appears as a continuation of first cycle (**Figures 11b** and **c**). Relaxation of ZFC magnetization with temperature quenching confirms the existence of memory effects in Co_2MnO_4 nanoparticles. A noticeable wait-time (t_{wt}) dependence of magnetization relaxation (*aging*) at 50 K in both M_{ZFC} and M_{FC} was noticed in these Co_2MnO_4 nanoparticles, which further supports the presence of the spin-glass behavior observed in this system.

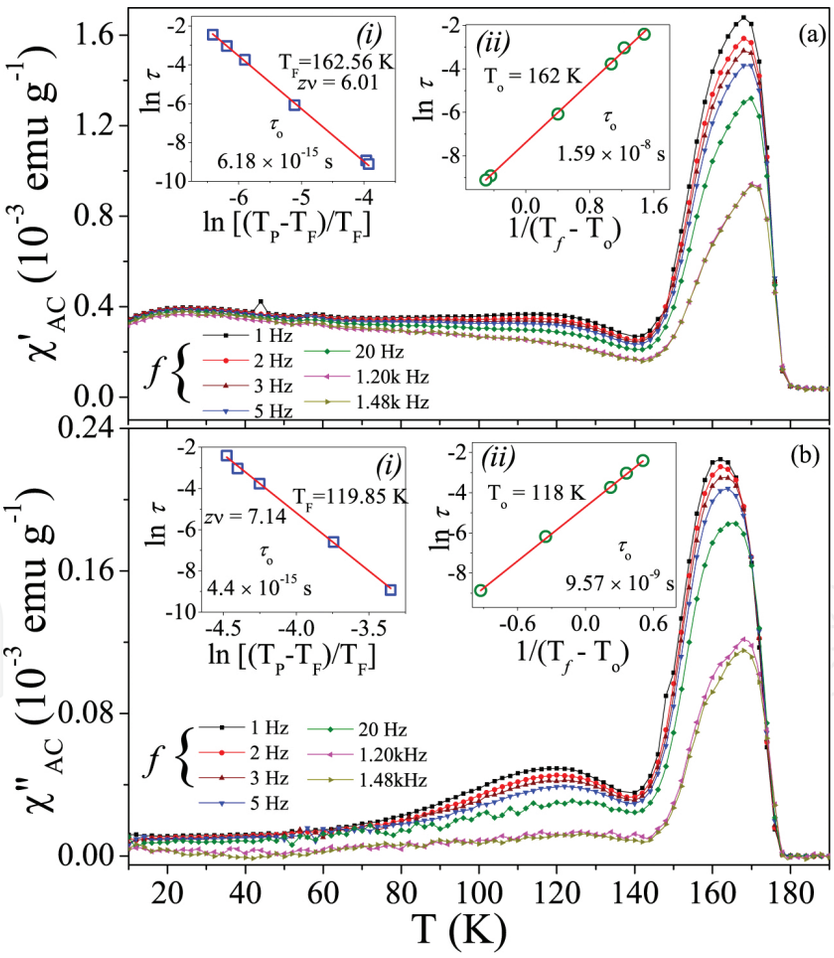

Figure 10. The real and imaginary components of the ac-magnetic susceptibilities ($\chi'(T)$ and $\chi''(T)$) of Co_2MnO_4 nanoparticles measured at various frequencies. The insets a(i) and b(i) represent the Vogel-Fulcher law whereas the insets a(ii) and b(ii) represent the power law of critical slowing down for both the peaks T_1 and T_2.

http://dx.doi.org/10.5772/65913

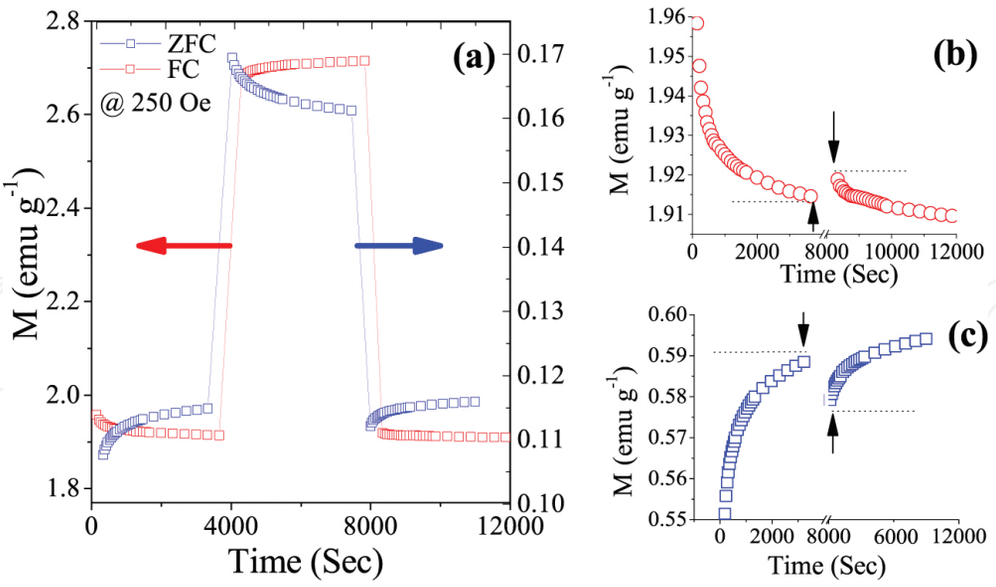

Figure 11. Magnetization relaxation $M(t)$ under ZFC and FC protocols with a temperature quench to 70 K at H = 250 Oe. The continuation of the first and third relaxation process during (b) ZFC and (c) FC cycles.

The high-temperature inverse magnetic susceptibility ($1/\chi_{ZFC}$ versus T) data of Co_2MnO_4 nanoparticles (**Figure 12**) fit well with the Néel's expression for ferrimagnets:

$$\frac{1}{\chi} = \frac{T}{C} + \frac{1}{\chi_0} - \left[\frac{\sigma_0}{T-\theta}\right] \tag{6}$$

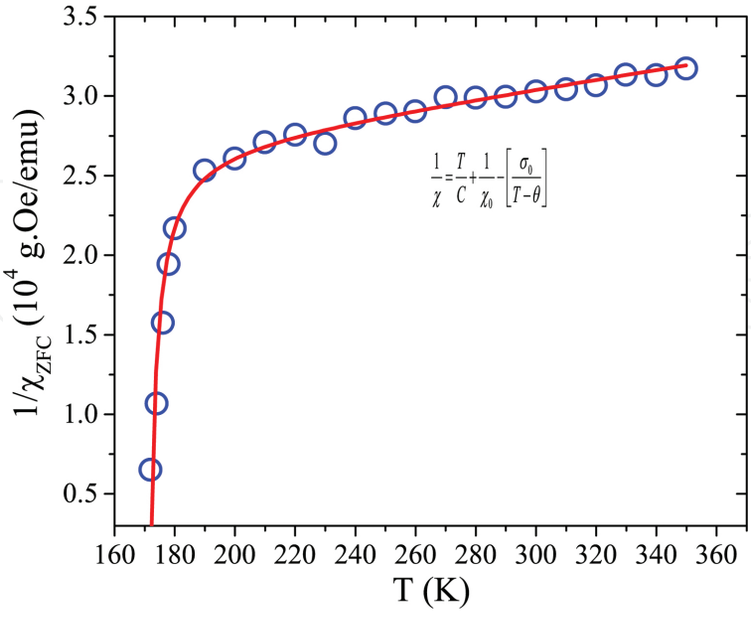

Figure 12. The scattered data represent the high-temperature inverse magnetic susceptibility ($1/\chi_{ZFC}$ versus T) of Co_2MnO_4 nanoparticles and the solid line represents the best fit to the Néel's expression for ferrimagnets Eq (6).

The fit (red line in **Figure 12**) yields: C = 0.0349 emu K/g Oe, χ_0 = 4.5 × 10^{-5} emu/g Oe, σ_0 = 5.76 × 10^4 g Oe K/emu, θ = 169.8 K, and the asymptotic Curie temperature $T_a = C/\chi_0$ = 775.6 K [90, 91]. T_a gives us information about the strength of antiferromagnetic exchange coupling between Mn^{3+} and Mn^{4+} at octahedral sites. Moreover, the effective magnetic moment μ_{eff} calculated using expression: $C = \frac{N\mu_{eff}^2}{3k_B}$ turnouts to be 8.13 μ_B.

5. Concluding remarks

In this review, magnetic properties of bulk and nanoparticles of the Co-based spinels Co_3O_4, Co_2SnO_4, Co_2TiO_4, and Co_2MnO_4 have been summarized. The fact that the observed magnetic properties of these spinels are so different is shown to result from the different occupation of the cations on the A- and B-sites and their different electronic states at these sites. The richness of the properties of spinels thus results from these differences.

Acknowledgements

The authors thank Prof. M. S. Seehra for his suggestions and guidance in organizing this chapter. Sobhit Singh acknowledges the support from the West Virginia University Libraries under OAAF program.

Author details

Subhash Thota[1*] and Sobhit Singh[2]

*Address all correspondence to: subhashiitk@gmail.com

1 Department of Physics, Indian Institute of Technology, Assam, India

2 Department of Physics & Astronomy, West Virginia University, Morgantown, USA

References

[1] A. Goldman, Magnetic Components for Power Electronics, Springer (Nov. 2001).

[2] D. W. Bruce, Functional Oxides, Wiley (2010).

[3] R. Padam, S. Pandya, S. Ravi, A. K. Nigam, S. Ramakrishnan, A. K. Grover, and D. Pal, Appl. Phys. Lett. 102, 112412 (2013).

[4] K. De Stropper, C. Henriet-Iserentant, G. Robbrecht, and V. Brabers, C. R. Acad. Sci. Ser. B 277, 75 (1973).

[5] W. L. Roth, J. Phys. Chem. Sol. 25, 1 (1964).

[6] P. Dutta, M.S. Seehra, S. Thota and J. Kumar, J. Phys. Condens. Matter, 20, 015218 (2008).

[7] S. Gangopadhyay, G. C. Hadjipanayis, C. M. Sorensen, and K. J. Klabunde, J. Appl. Phys. 73, 6964 (1993).

[8] D. A. Resnick, K. Gilmore, Y. U. Idzerda, M. T. Klem, M. Allen, T. Douglas, E. Arenholz, and M. Young, J. Appl. Phys. 99, 08Q501 (2006).

[9] L. He, C. Chen, N. Wang, W. Zhou, and L. Guo, J. Appl. Phys. 102, 103911 (2007).

[10] E. L. Salabas, A. Rumplecker, F. Kleitz, F. Radu and F. Schuth, Nano. Lett. 6, 2977 (2006).

[11] M. Andok, T. Kobayashi, S. Iijima and M. Haruta, J. Mater. Chem. 7, 1779 (1997).

[12] H. Yamaura, J. Tamaki, K. Moriya, N. Miura and N. Yamazoe, J. Electrochem. Soc. 144, L158 (1997).

[13] P. Nkeng, J. Koening, J. Gautier, P. Chartier and G. Poillerat, J. Electroanal. Chem. 402, 81 (1996).

[14] S. G. Chrisoskova, M. Stoyanova, M. Georgieva and D. Mehandjiev, Mater. Chem. Phys. 60, 39 (1999).

[15] M. M. Natile and A. Glisenti, Chem. Mater. 14, 3090 (2002).

[16] T. Maruyama and S. Arai, J. Electrochem. Soc. 143, 1383 (1996).

[17] G. B. Smith, A. Ignatiev and G. Zajac, J. Appl. Phys. 51, 4186 (1980).

[18] K. Chidambaram, K. L. Malhotra and K. L. Chopra, Thin Solid Films 87, 365 (1982).

[19] L. M. Khriplovich, E. V. Kholopov and I. E. Paukov, J. Chem. Thermodyn. 14, 207 (1982).

[20] M. E. Fisher, Philos. Mag. 7, 1731 (1962).

[21] D. Sherrington and S. Kirkpatrick, Phys. Rev. Lett. 35, 1792 (1975).

[22] A. J. Bray and G. J. Rodgers, Phys. Rev. B, 38, 9252 (1988); A. J. Bray, Phys. Rev. Lett. 60, 720 (1988).

[23] M. Gabay and G. Toulouse. Phys. Rev. Lett. 47, 201 (1981); J. Villain, Z. Phys. B 33, 31 (1979).

[24] E. Harmon, D. J. Simkin, R. J. Haddad, and W. B. Muir, J. Phys. Colloq. 38, CI–131 (1977); AIP Conf. Proc. 29, 576 (1976).

[25] J. Srivastava and J. Kulkarni, J. Phys. C: Solid State Phys. 20, 2139 (1987).

[26] B. Antic, G. Goya, H. Rechenberg, V. Kusigerski, N. Jovic, and M. Mitric, J. Phys. Condens. Matter 16, 651 (2004).

[27] S. Thota, V. Narang, S. Nayak, S. Sambasivam, B.C. Choi, T. Sarkar, M. S. Andersson, R. Mathieu, and M. S. Seehra, J. Phys.Condens. Matter, 27, 166001 (2015)

[28] J. K. Srivastava et al., J. Appl. Phys. 61, 3622 (1987).

[29] K. De Strooper, Phys. Stat. Sol. A 39, 431 (1977).

[30] I. Mihailova, L. Radev, and D. Mehandjiev, Oxid. Commun. 35, 58 (2012).

[31] J. Hubsch and G. Gavoille, Phys. Rev. B 26, 3815 (1982).

[32] N. Sakamoto and Y. Yamaguchi, J. Phys. Soc. Jpn. 17, 276 (1962).

[33] S. Nayak, S. Thota, D. C. Joshi, M. Krautz, A. Waske, A. Behler, J. Eckert, T. Sarkar, M. S. Andersson, R. Mathieu, V. Narang, and M. S. Seehra, Phys. Rev. B 92, 214434 (2015).

[34] G. Gavoille, J. Hubsch, and S. Koutani, J. Magn. Magn. Mater. 102, 283 (1991).

[35] K. De Strooper and G. Robbrecht, Physica B 86, 934 (1977).

[36] S. Ogawa and S. Waki, J. Phys. Soc. Jpn. 20, 540 (1965).

[37] K. De Strooper, A. Govaert, C. Dauwe, and G. Robbrecht, Phys. Stat. Sol. A 37, 127 (1976).

[38] S. Thota and M. S. Seehra, J. Appl. Phys. 118, 129901 (2015).

[39] V. Sagredo, B. Watts and B. Wanklyn, J. Phys. IV France 7, C1-279 (1997).

[40] S. Thota and M. S. Seehra, J. Appl. Phys. 113, 203905 (2013).

[41] R. L. Stamps, J. Phys. D: Appl. Phys. 33, R247 (2000).

[42] W. H. Meiklejohn and C. P. Bean, Phys. Rev. 102, 1413 (1956).

[43] M. Ali, P. Adie, C. H. Marrows, D. Greig, B. J. Hickey, and R. L. Stamps, Nat. Mater. 6, 70 (2007).

[44] W. C. Cain and M. H. Kryder, J. Appl. Phys. 67, 5722 (1990).

[45] G. S. Alvarez, J. Sort, S. Surinach, M. D. Baro, and J. Nogues, J. Am. Chem. Soc. 129, 9102 (2007).

[46] W. H. Meiklejohn, J. Appl. Phys. 33, 1328 (1962).

[47] A. Punnoose, M. S. Seehra, J. Van Tol, and L. C. Brunel, J. Magn. Magn. Mater. 288, 168 (2005).

[48] B. M. Wang, Y. Liu, P. Ren, B. Xia, K. B. Ruan, J. B. Yi, J. Ding, X. J. Li, and L. Wang, Phys. Rev. Lett. 106, 077203 (2011).

[49] A. K. Nayak, M. Nicklas, S. Chadov, C. Shekhar, Y. Skourski, J. Winterlik, and C. Felser, Phys. Rev. Lett. 110, 127204 (2013).

[50] A. K. Nayak, M. Nicklas, S. Chadov, P. Khuntia, C. Shekhar, A. Kalache, et al, Nat. Mater. 14, 679, (2015).

[51] K. Guduru, A. Puri, U. Zeitler, J. M. D. Coey and C. Felser, Nat. Mater. 14, 679 (2015).

[52] F. C. Romeijn, Philips. Res. Rep. 8, 304 (1953).

[53] S. Nayak, D. C. Joshi, M. Krautz, A. Waske, J. Eckert and S. Thota, J. Appl. Phys. 119, 043901 (2016).

[54] H. Wang, Y. Yang, Y. Liang, G. Zheng, Y. Li, Y. Cui and Hongji, Energy Environ. Sci. 5, 7931 (2012).

[55] R. Alcantara, M. Jaroba, P. Lavela and J. L. Tirado, Chim. Mater. 1, S108 (2002).

[56] P. Umadevi and C. L. Nagendra, Sens. Actuator A Phys. 96, 114 (2002).

[57] Y. Shimizu and M. Shiotsuka, Jpn. J. Appl. Phys. 41, 6243 (2003).

[58] N. Nagatomo, K. Eudo and T. Yonezawa, Key Eng. Mater. 159/160, 305 (1999).

[59] E. Jabrya, A. Roussetb and A. Lagrange, Phase Trans 13, 13 (1988).

[60] Xiaoming Ge, Yayuan Liu, F. W. Thomas Goh, T. S. Andy Hor, Yun Zong, Peng Xiao, et al. ACS Appl. Mater. Interfaces 6, 12684 (2014).

[61] G. N. Pirogova, N. M. Panich, R. J. Korosteleva, Y. V. Voronin and N. N. Popova, Russ. Chem. Bull. 49, 1536 (2000).

[62] T. Nissinen, Y. Kiros, M. Gasik and M. Lampinen, Mater. Res. Bull. 39, 1195 (2004).

[63] J. Li, S. Xiong, X. Li and Y. Qian, Nanoscale 5, 2045 (2013).

[64] T. Nguyen, M. Boudard, L. Rapenne, O. Chaix-Pluchery, M. João Carmezim and M. F. Montemor, RSC Adv. 5, 27844 (2015).

[65] A. D. Sharma, J. Mukhopadhaya and R. N. Basu, ECS Trans. 35, 2509 (2011).

[66] Y. Xu, Z. Wen, S. Wang and T. Wen, Solid State Ion. 192, 561 (2011).

[67] J. Philip and T. R. N Kutty, Mater. Lett. 39, 311 (1999).

[68] F. K. Lotgering, Philip Res. Rep. 11, 337 (1956).

[69] E. Ríos, O. Peña, T. Guizouarn and J.-L. Gautier, Phys. Stat. Sol. C 1, S108 (2004).

[70] P. A. Joy and S. K. Date, J. Magn. Magn. Mater. 210, 31 (2000).

[71] S. Tamura, J. Phys. Soc. Jpn. 61, 752 (1992).

[72] D. G. Wickham and W. J. Croft, J. Phy. Chem. Sol. 7, 351 (1958).

[73] G. Blasse, Philip Res. Rep. Suppl. 18, 383 (1963).

[74] E. Ríos, P. Lara, D. Serafini, A. Restovic and J. L. Gautier, J. Chil. Chem. Soc. 55, 261 (2010).

[75] B. Boucher, R. Bhul, R. Di Bella and M. Perrin, (Paris) J. Phys. 31, 113 (1970).

[76] N. Yamamoto, S. Higashi, S. Kawano and N. Achiwa, J. Mater. Sci. Lett. 2, 525 (1983).

[77] J. L. Gautier, S. Barbato and J. Brenet, C. R. Acad. Sci. Paris 294, 427 (1982).

[78] J. L. Gautier and C. Cabezas, J. Electroanal. Chem. 159, 137 (1983).

[79] A. Restovic, E. Ríos, S. Barbato, J. Ortiz and J. L. Gautier, J. Electroanal. Chem. 522, 141 (2002).

[80] I. Aoki, J. Phys. Soc. Jpn. 17, 1 (1962).

[81] J. L. Gautier, E. Ríos, M. Gracia, J. F. Marco and J. R. Gancedo, Thin Solid Films. 311, 51 (1997).

[82] S. Trasatti, Electrochim. Acta 36, 225 (1991).

[83] G.V. Bazuev and A.V. Korolyov, J. Magn. Magn. Mater. 320, 2262 (2008).

[84] F. M. M. Borges, D. M. A. Melo, M. S. A. Camera, A. E. Martinelli, J. M. Soares, J. H. De Araujo and F. A. O. Cabral, J. Magn. Magn. Mater. 302, 273 (2006).

[85] J. L. Snoek, Physica 8, 426 (1941).

[86] C. Heck, Magnetic Materials and their Applications, Butterworths, London, p. 147 (1974).

[87] S. Senoussi, J. Phys. 45, 315 (1984).

[88] J. Smit and H. P. J. Wijin, Les ferrites, Bibl. Tech. Philips, Paris, (1961).

[89] S. Thota, S. K. Das, A. Kumar, S. Sangaraju and B. C. Choi, IEEE Trans. Magn. 49, 3 (2013).

[90] G. Srinivasan and M. S. Seehra, Phys. Rev. B 28, 1 (1983).

[91] S. K. Singh, M. S. Seehra and S. Thota, APS March Meeting Abstracts 1, 1284 (2013).